OPTIMIZATION-BASED COMPARISON OF DIFFERENT APPROACHES FOR THE AUTOMATIZED CALCULATION OF RESIDUAL STRESSES AND FIBER ORIENTATIONS IN ARTERIES

ANNA ZAHN[*†] AND DANIEL BALZANI[†]

[†]Chair of Continuum Mechanics, Department of Civil and Environmental Engineering,
Ruhr-Universität Bochum, Universitätsstraße 150, 44801 Bochum, Germany
e-mail: anna.zahn@ruhr-uni-bochum.de, daniel.balzani@ruhr-uni-bochum.de

Key words: Arterial Walls, Stress-driven Growth and Fiber Reorientation, Optimization

Abstract. Residual stresses and fiber orientations in arterial walls can be approximated by means of the simulation of growth and remodeling processes. In order to enable a comparison of different approaches of combined growth and remodeling in one framework, a method based on the optimization of model parameters is developed. The minimization of a mechano-biologically motivated objective function permits to evaluate the approaches with respect to their ability of effectively reducing stress peaks and stress inhomogeneities in the arterial wall. This examination is performed for a simplified, one-layered, rotationally symmetric arterial segment in order to enable the analysis of the fundamental mechanisms included in the individual model variants. Once the most probable growth mechanism is identified, multi-layered segments can be analyzed in more detail.

1 INTRODUCTION

The mechanical behavior of arterial tissues is considerably affected by residual stresses, which reduce stress peaks and gradients in the arterial wall [8, 9]. Furthermore, the arrangement of the collagen fibers, whose orientation is graded over the wall thickness, strongly affects the load bearing behavior. Unfortunately, residual stresses or fiber orientations can currently hardly be measured in vivo. However, they have to be known in order to perform reliable patient-specific numerical simulations. Both phenomena can be included by modeling the adaptation of the artery to its mechano-biological environment, which appears as arterial growth and remodeling.

Following Hariton et al. [6], it is assumed that the collagen fibers reorient based on the principal stress state such that they arrange symmetrically with respect to the principal axes. The reorientation towards the target fiber orientations is here described by an evolution equation, which assures that abrupt changes do not occur.

If growth is simulated in tubular structures, residual stresses arise automatically as a consequence of the growth deformation and need not to be taken into account for instance by rather technical approaches as e. g. presented by Balzani et al. [2] or Schröder and von Hoegen [13]. The growth model applied here is based on a multiplicative decomposition of the deformation gradient into an elastic and a growth part as originally proposed by Rodriguez et al. [12] and then pursued amongst others by Kuhl et al. [10] or Göktepe et al. [5]. In order to account for the anisotropy of the growth mechanism, the growth part itself is decomposed here into up to three individual parts, where each part is associated to a principal direction of a stress tensor. By specifying the number and form of the individual growth tensors and by using different growth-driving quantities, a set of different formulations for the automatized calculation of residual stresses and fiber orientations is obtained. A detailed description of the combined growth and remodeling framework has been published in [14].

This contribution aims at developing a method which enables a quantitative comparison of the fundamental mechanisms included in the different formulations. The growth parameters are therefore computed by minimizing a mechano-biologically motivated objective function, which is formulated such that its minimum reflects the most efficient reduction of stress peaks and stress inhomogeneities in the arterial layers. This systematic analysis is conducted for different loading scenarios applied to a simplified one-layered artery which is idealized as a rotationally symmetric tube, enabling an efficient optimization. By comparing the obtained minima of the individual approaches, an assessment regarding the most probable mechano-biological mechanism is enabled.

2 GROWTH AND REMODELING FRAMEWORK

As initially proposed in [12], the growth model is based on the multiplicative decomposition $\boldsymbol{F} = \boldsymbol{F}_{\mathrm{e}}\boldsymbol{F}_{\mathrm{g}}$ of the deformation gradient into a pure growth part $\boldsymbol{F}_{\mathrm{g}}$, which involves a stress-free volume change of factor $J_{\mathrm{g}} = \det[\boldsymbol{F}_{\mathrm{g}}]$, and a remaining elastic part $\boldsymbol{F}_{\mathrm{e}}$, which generates stresses. The 2$^{\mathrm{nd}}$ Piola-Kirchhoff stress tensor is obtained as $\boldsymbol{S} = \boldsymbol{F}_{\mathrm{g}}^{-1}\boldsymbol{S}_{\mathrm{e}}\boldsymbol{F}_{\mathrm{g}}^{-T}$, where $\boldsymbol{S}_{\mathrm{e}} = 2\,\partial\psi/\partial\boldsymbol{C}_{\mathrm{e}}$ is the stress in the intermediate configuration, which is defined by an appropriate strain energy function ψ and arises from the deformation tensor $\boldsymbol{C}_{\mathrm{e}} = \boldsymbol{F}_{\mathrm{e}}^{T}\boldsymbol{F}_{\mathrm{e}} = \boldsymbol{F}_{\mathrm{g}}^{-T}\boldsymbol{C}\boldsymbol{F}_{\mathrm{g}}^{-1}$. A polyconvex hyperelastic strain energy function from [1] is used to describe the orthotropic material behavior. It takes two families of fibers into account, whose orientations are given by the vectors $\boldsymbol{A}^{(1)}$ and $\boldsymbol{A}^{(2)}$.

2.1 General framework

Accounting for the orthotropic behavior of soft biological tissues, the growth tensor itself is decomposed into three parts according to

$$\boldsymbol{F}_{\mathrm{g}} = \boldsymbol{F}_{\mathrm{g}}^{(3)}\boldsymbol{F}_{\mathrm{g}}^{(2)}\boldsymbol{F}_{\mathrm{g}}^{(1)}, \tag{1}$$

where each part is related to one of three perpendicular directions $\boldsymbol{A}_{\mathrm{g}}^{(a)}$ and an internal variable $\vartheta^{(a)}$, $a = 1, 2, 3$, determining the amount of growth. For the definition of the parts of the growth tensor, it is supposed that growth is a stress-driven process which

aims at reducing high stress values [4]. The directions $\boldsymbol{A}_{\mathrm{g}}^{(a)}$ are therefore not meant to represent coordinate axes or structural directions, but rather refer to the local stress state of the tissue. Assuming that all growth and remodeling processes are driven by the same stress quantity, the elastic part of the Mandel stress tensor, i.e. $\boldsymbol{C}_{\mathrm{e}}\boldsymbol{S}_{\mathrm{e}} =: \boldsymbol{\Sigma}_{\mathrm{e}}$, is chosen as driving quantity as proposed in [7] and the directions $\boldsymbol{A}_{\mathrm{g}}^{(a)}$ are computed as principal directions of this stress tensor. The evolution of the growth factors $\vartheta^{(a)}$ is described by a coupled set of evolution equations

$$\dot{\vartheta}^{(a)} = k_{\vartheta}^{(a)}(\vartheta^{(a)})\,\phi^{(a)}(\boldsymbol{\Sigma}_{\mathrm{e}}), \qquad a = 1, 2, 3, \tag{2}$$

which is also formulated in dependence on the elastic part of the Mandel stress. Besides the growth function $k_{\vartheta}^{(a)}$ from [11] with

$$k_{\vartheta}^{(a)}(\vartheta^{(a)}) = \begin{cases} k_{\vartheta,(a)}^{+} \left[\dfrac{\vartheta_{(a)}^{+} - \vartheta^{(a)}}{\vartheta_{(a)}^{+} - 1} \right]^{m_{\vartheta,(a)}^{+}} & \text{for} \quad \phi^{(a)} > 0 \\[2em] k_{\vartheta,(a)}^{-} \left[\dfrac{\vartheta^{(a)} - \vartheta_{(a)}^{-}}{1 - \vartheta_{(a)}^{-}} \right]^{m_{\vartheta,(a)}^{-}} & \text{for} \quad \phi^{(a)} < 0 \\[2em] 0 & \text{for} \quad \phi^{(a)} = 0, \end{cases} \tag{3}$$

a driving force $\phi^{(a)}$ is involved for each direction a. The algorithmic implementation of the growth model within a finite element framework is explained in detail in [14].

The fiber orientation vectors $\boldsymbol{A}^{(1)}$ and $\boldsymbol{A}^{(2)}$ are considered as variable, adjusting automatically following local demands. Once again, the elastic part of the Mandel stress tensor is used to define this reorientation process. Following the hypothesis in [6], the load-bearing behavior can be improved if the fibers arrange symmetrically with respect to the tensile principal stresses and if their orientation within the plane of the highest tensile principal stresses is governed by the ratio of these stresses. The target fiber orientation vectors are thus defined by

$$\bar{\boldsymbol{A}}_{\mathrm{targ}}^{(1)} = \langle \Sigma_{\mathrm{e}}^{\mathrm{I}} \rangle \boldsymbol{e}_{\mathrm{I}} + \langle \Sigma_{\mathrm{e}}^{\mathrm{II}} \rangle \boldsymbol{e}_{\mathrm{II}} \qquad \text{and} \qquad \bar{\boldsymbol{A}}_{\mathrm{targ}}^{(2)} = \langle \Sigma_{\mathrm{e}}^{\mathrm{I}} \rangle \boldsymbol{e}_{\mathrm{I}} - \langle \Sigma_{\mathrm{e}}^{\mathrm{II}} \rangle \boldsymbol{e}_{\mathrm{II}}, \tag{4}$$

where $\boldsymbol{e}_{\mathrm{I}}$ and $\boldsymbol{e}_{\mathrm{II}}$ are unit vectors in the directions of the principal stresses $\Sigma_{\mathrm{e}}^{\mathrm{I}}$ and $\Sigma_{\mathrm{e}}^{\mathrm{II}}$ of the elastic part of the Mandel stress. Use of the Macaulay brackets, which are defined as $\langle \bullet \rangle = \frac{1}{2}\left(|\bullet| + \bullet \right)$, guarantees that only positive principal stresses are included. Since the constitutive equations are formulated in the reference configuration, the target vectors are pulled back and optionally exchanged and/or rotated by $180°$ to keep the remodeling effort minimal. Finally, the vectors $\boldsymbol{A}_{\mathrm{targ}}^{(1)}$ and $\boldsymbol{A}_{\mathrm{targ}}^{(2)}$ are obtained as target vectors for the fiber orientation vectors $\boldsymbol{A}^{(1)}$ and $\boldsymbol{A}^{(2)}$. The numerical treatment of the reorientation process is handled as described in [14], making use of an evolution equation $\dot{\eta}^{(a)} = k_{\eta}(\eta^{(a)})$ for each fiber family. Herein, the variable $\eta^{(a)}$ represents the angle between $\boldsymbol{A}^{(a)}$ and $\boldsymbol{A}_{\mathrm{targ}}^{(a)}$ and the remodeling function $k_{\eta}(\eta^{(a)}) = -k_{\eta}^{+}\ln(m_{\eta}^{+}|\eta^{(a)}| + 1)$ (with $\eta^{(a)}$ in rad) defines the temporal behavior.

2.2 Variability of model components

So far, the individual parts of the growth tensor in Eq. (1) and the driving forces for the evolution of the growth factors in Eq. (2) have not been specified in detail. Both can be chosen based on hypotheses on the mechanism of growth and stress reduction, but nevertheless, a variety of different approaches is imaginable. The purpose of this contribution is to develop a method which enables an optimization-based comparison of these approaches, such that finally an estimation regarding the most probable mechanism is possible. Thereby, the focus is however rather on the anisotropic character of growth than on bio-chemical aspects.

Concerning the form of the individual parts $\boldsymbol{F}_{\mathrm{g}}^{(a)}$ of the growth tensor, three different approaches, namely

$$\boldsymbol{F}_{\mathrm{g}}^{(a)} = \vartheta^{(a)} \boldsymbol{I}, \tag{5a}$$

$$\boldsymbol{F}_{\mathrm{g}}^{(a)} = \vartheta^{(a)} \boldsymbol{I} + \left(1 - \vartheta^{(a)}\right) \boldsymbol{A}_{\mathrm{g}}^{(a)} \otimes \boldsymbol{A}_{\mathrm{g}}^{(a)}, \tag{5b}$$

$$\boldsymbol{F}_{\mathrm{g}}^{(a)} = \boldsymbol{I} + \left(\vartheta^{(a)} - 1\right) \boldsymbol{A}_{\mathrm{g}}^{(a)} \otimes \boldsymbol{A}_{\mathrm{g}}^{(a)}, \tag{5c}$$

are included to the examination. The first approach in Eq. (5a) describes isotropic growth. Due to the anisotropy of arterial tissues, isotropic growth is expected not to be a realistic model assumption. Therefore, the anisotropic forms in Eqs. (5b) and (5c) are additionally taken into account. They describe growth perpendicular to a direction $\boldsymbol{A}_{\mathrm{g}}^{(a)}$ as well as growth in a direction $\boldsymbol{A}_{\mathrm{g}}^{(a)}$, respectively. Depending on the type of loading, both mechanisms can effectively reduce stresses in the direction of $\boldsymbol{A}_{\mathrm{g}}^{(a)}$, either by an increase of the cross-sectional area or by an elongation in the direction of the load.

For the driving force governing the evolution of the growth factors $\vartheta^{(a)}$, the set of approaches chosen for the examination is given by

$$\phi^{(a)}(\boldsymbol{\Sigma}_{\mathrm{e}}) = \boldsymbol{\Sigma}_{\mathrm{e}} : \boldsymbol{I}, \tag{6a}$$

$$\phi^{(a)}(\boldsymbol{\Sigma}_{\mathrm{e}}) = \boldsymbol{\Sigma}_{\mathrm{e}} : \boldsymbol{M}_{\mathrm{g}}^{(a)}, \tag{6b}$$

$$\phi^{(a)}(\boldsymbol{\Sigma}_{\mathrm{e}}) = \left\langle \boldsymbol{\Sigma}_{\mathrm{e}} : \boldsymbol{M}_{\mathrm{g}}^{(a)} \right\rangle, \tag{6c}$$

$$\phi^{(a)}(\boldsymbol{\Sigma}_{\mathrm{e}}) = \begin{cases} \frac{1}{2} \boldsymbol{\Sigma}_{\mathrm{e}} : \left(\boldsymbol{M}_{\mathrm{g}}^{(\mathrm{I})} + \boldsymbol{M}_{\mathrm{g}}^{(\mathrm{II})}\right) & \text{for} \quad \Sigma_{\mathrm{e}}^{\mathrm{I}} > 0, \quad \Sigma_{\mathrm{e}}^{\mathrm{II}} > 0 \\ \boldsymbol{\Sigma}_{\mathrm{e}} : \boldsymbol{M}_{\mathrm{g}}^{(\mathrm{I})} & \text{for} \quad \Sigma_{\mathrm{e}}^{\mathrm{I}} > 0, \quad \Sigma_{\mathrm{e}}^{\mathrm{II}} \leq 0 \end{cases}, \tag{6d}$$

where $\boldsymbol{M}_{\mathrm{g}}^{(\bullet)} = \boldsymbol{A}_{\mathrm{g}}^{(\bullet)} \otimes \boldsymbol{A}_{\mathrm{g}}^{(\bullet)}$. The indices I and II point out that the 1st and 2nd principal directions of $\boldsymbol{\Sigma}_{\mathrm{e}}$ are referred to. Besides the isotropic stress measure in Eq. (6a), a projection of the elastic part of the Mandel stress in the direction of $\boldsymbol{A}_{\mathrm{g}}^{(a)}$ is considered as driving force in Eq. (6b). Furthermore, the case that only positive values of these projected stresses, i. e. tensile stresses, provoke growth, is reflected in Eq. (6b). In addition, Eq. (6d) represents the average stress state within the plane spanned by the fiber families. In the case of only one tensile principal stress, the stress projected in the associated direction is used and both fiber families align in this direction, cf. Eq. (4).

In order to allow for a concise denomination of the different approaches, the numeric identifiers "$\boldsymbol{F}_{\mathrm{g}}$-ID" and "$\phi$-ID" are introduced for the type of growth tensor and the type of driving force, respectively. Their values are summarized in Tables 1 and 2. Note that it is not necessary to include each of the three parts of $\boldsymbol{F}_{\mathrm{g}}$. Purely isotropic growth for instance is already defined by setting $\boldsymbol{F}_{\mathrm{g}} = \boldsymbol{F}_{\mathrm{g}}^{(1)} = \vartheta^{(1)}\boldsymbol{I}$. The number of included directions will be referred to as n_{dir} in the following.

Table 1: Denomination of the different forms of the individual parts of the growth tensor.

$\boldsymbol{F}_{\mathrm{g}}$-ID	type of growth	$\boldsymbol{F}_{\mathrm{g}}^{(a)}$
1	isotropic growth	Eq. (5a)
2	growth perpendicular to $\boldsymbol{A}_{\mathrm{g}}^{(a)}$	Eq. (5b)
4	growth in the direction of $\boldsymbol{A}_{\mathrm{g}}^{(a)}$	Eq. (5c)

Table 2: Denomination of the different driving forces.

ϕ-ID	type of driving force	$\phi^{(a)}$
2	isotropic stress measure	Eq. (6a)
4	stress in the direction of $\boldsymbol{A}_{\mathrm{g}}^{(a)}$	Eq. (6b)
5	stress within the plane of the fibers	Eq. (6d)
6	tensile stress in the direction of $\boldsymbol{A}_{\mathrm{g}}^{(a)}$	Eq. (6c)

3 OPTIMIZATION-BASED COMPARISON OF THE APPROACHES

With the high number of adjustable model components listed above, a multitude of different approaches can be generated. A comparison of these approaches is made even more difficult by the dependence of their behavior on the growth and remodeling parameters. Most of these parameters however mostly affect the velocity of the adaptation processes and not the final result. Provided that a growth equilibrium state is attained, the resulting stress distributions are supposed to mainly depend on the form of the individual parts $\boldsymbol{F}_{\mathrm{g}}^{(a)}$ of the growth tensor, the associated driving forces $\phi^{(a)}$ and the limiting values $\vartheta_{(a)}^{+}$ of the growth factors for positive growth. In order to compare different approaches, these parameters have to be set specifically such that the best possible behavior in a biomechanical sense is achieved. This is done by optimization of a mechano-biologically motivated objective function, which then also serves as comparative value between the approaches.

3.1 Growth equilibrium state

Before evaluating the objective function, it has to be assured that a growth equilibrium state is attained after application of the load. Such a state is indicated by a vanishing

rate of all growth factors and is thus assumed to be attained if the condition

$$\frac{1}{n_{\text{ele}}\, n_{\text{GP}}\, n_{\text{dir}}} \sum_{n_{\text{ele}}} \sum_{n_{\text{GP}}} \sum_{a=1}^{n_{\text{dir}}} \frac{\left|\vartheta_{t+\Delta t}^{(a)} - \vartheta_t^{(a)}\right|}{\vartheta_t^{(a)} \Delta t} < \epsilon \tag{7}$$

is fulfilled. Thereby n_{ele} and n_{GP} are the numbers of elements and Gauß points and ϵ is set to $\epsilon = 10^{-4}/\text{s} = 0.01\,\%/\text{s}$. At growth equilibrium, a final stress state is reached which is used for the evaluation of the objective function.

3.2 Definition of the objective function

For the purpose of evaluating different growth mechanisms with respect to their ability of efficiently improving the load-bearing behavior, an objective function of the structure

$$f_{\text{obj}} = \sum_i \omega_i\, q_i \tag{8}$$

is defined, where q_i are the arguments and ω_i are weighting factors representing the importance of the individual arguments. The arguments q_i denote optimization objectives which are claimed to be minimal at growth equilibrium, for example stress peaks or differences and the volume change due to growth. All these objectives are normalized such that they are unitless and of same order of magnitude, and their optimal value is zero. By minimizing Eq. (8), the specific set of parameters is obtained that leads to the optimal mechano-biological state reachable by the particular model variant. The explicit expressions are

$$q_1 = \frac{\max\limits_{r} |\sigma_\varphi|}{\tilde{\sigma}_{\text{peak}}}, \qquad\qquad q_4 = \frac{\max\limits_{r} |\sigma_\varphi| - \left|\max\limits_{r} \sigma_\varphi\right|}{\tilde{\sigma}_{\text{diff}}},$$

$$q_2 = \frac{\max\limits_{r} |\sigma_z|}{\tilde{\sigma}_{\text{peak}}}, \qquad\qquad q_5 = \frac{\max\limits_{r} |\sigma_z| - \left|\max\limits_{r} \sigma_z\right|}{\tilde{\sigma}_{\text{diff}}}, \tag{9}$$

$$q_3 = \frac{\max\limits_{r} |\sigma_\varphi - \sigma_z|}{\left|\max\limits_{r} \sigma_\varphi\right|}, \qquad\qquad q_6 = \left|\max\limits_{\mathcal{B}} J_{\text{g}} - 1\right|,$$

where the stresses $\tilde{\sigma}_{\text{peak}}$ and $\tilde{\sigma}_{\text{diff}}$ are introduced as normalizing values for stress peaks and differences. The operator "mean" denotes the volume average of a quantity over the whole domain $\mathcal{B}$ or over the radial direction r, respectively. In a multi-layered model, a layer-wise examination of the means would be more reasonable. Here, the artery is assumed to consist of a single layer in order to keep the numerical effort low, which is justified since the fundamental mechanism is matter of interest. The mechano-biological motivation for the objective definitions above is as follows:

q_1: In a cylindrical tube with internal pressure and moderate axial strain, the highest stress occurs at the internal surface in circumferential direction. A reduction of this stress peak towards a reference level $\tilde{\sigma}_{\text{peak}}$ or less might therefore be desired by the tissue in order to increase its resilience.

q_2: The same might hold for the peak of the axial stress, which however can also become compressive in case of intense axial growth. For this reason, the absolute value is considered.

q_3: Healthy arteries cut from the body contract in axial direction, which means that their natural in vivo state is under axial tension. Zero axial stresses are thus not expected and a layer-wise reduction of the average difference between circumferential and axial stresses is potentially a more realistic goal of arterial adaptation.

q_4/q_5: To obtain stress distributions which are layer-wise constant over the wall thickness as far as possible, the maximal stresses per layer have to approach the mean values. Constant stresses might be desired since the material within a layer is assumed to prefer a uniform exposure that does only marginally vary over the radial position.

q_6: From an energetic point of view, the material is assumed to avoid an unnecessarily high amount of grown material, i.e. to keep the volume change induced by growth, $J_g - 1$, at the lowest level possible.

In the examination presented here, each of the optimization goals is supposed to be equally important, which means that all weighting factors are set to $\omega_i = 1$. The normalizing stresses are set to

$$\tilde{\sigma}_{\text{peak}} = 100\,\text{kPa} \qquad \text{and} \qquad \tilde{\sigma}_{\text{diff}} = 50\,\text{kPa}, \tag{10}$$

since these values are estimated to be in the order of magnitude of average stress peaks and differences between peak and mean values.

4 NUMERICAL EXAMINATION

The boundary value problem considered for the optimization-based comparison of different model approaches is a one-layered arterial segment discretized into seven rotationally symmetric 2D finite elements over the wall thickness, see Fig. 1. Table 3 lists all parameters which are set equally for all simulations. Besides the material parameters, this also applies to the remodeling parameters and to growth parameters with minor impact on the growth equilibrium state. The initial fiber angles are set to $\pm 30°$ with respect to the circumferential direction.
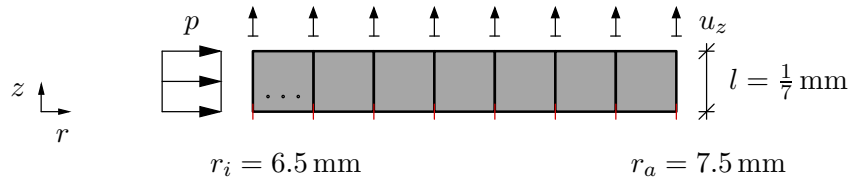

Figure 1: Boundary value problem of a rotationally symmetric arterial segment loaded by an internal pressure p and an axial displacement u_z.

Table 3: Parameters of the material model from [1], adjusted to human media in [3], parameters of the remodeling function k_η and unvaried parameters of the growth function $k_\vartheta^{(a)}$, set equally for all directions.

c_1	ϵ_1	ϵ_2	α_1	α_2	k_η^+	m_η^+	k_ϑ^+	m_ϑ^+	ϑ^-	k_ϑ^-	m_ϑ^-
in kPa	in kPa	in –	in kPa	in –	in s^{-1}	in –	in s^{-1}	in –	in –	in s^{-1}	in –
17.5	499.8	2.4	30 001.9	5.1	0.6	5.0	1.0	3.0	0.95	1.0	3.0

In a first simulation step, an internal pressure of $p = 120\,\text{mmHg}$ and an axial displacement u_z are applied without activating growth and remodeling. After reaching this representative loading, the load is kept constant and growth and remodeling are activated. The computation is then continued until a growth equilibrium state is attained.

To give an example for the values of the objective function in the non-growing reference artery, its stress state for an axial displacement of $u_z = 0.05\,l$ is given in Fig. 2 a and the associated contributions $\omega_i\,q_i$ as well as the summarized value f_obj are depicted in the bar plot in Fig. 2 b. Such a plot depicts the reachable performance of an individual model approach and thus, this case with $f_\text{obj} = 5.403$ where no growth and remodeling is considered, should indicate a relatively poor performance. However, note that the absolute values of the individual objectives themselves have few meaning and can only be evaluated by comparing them between different model approaches.
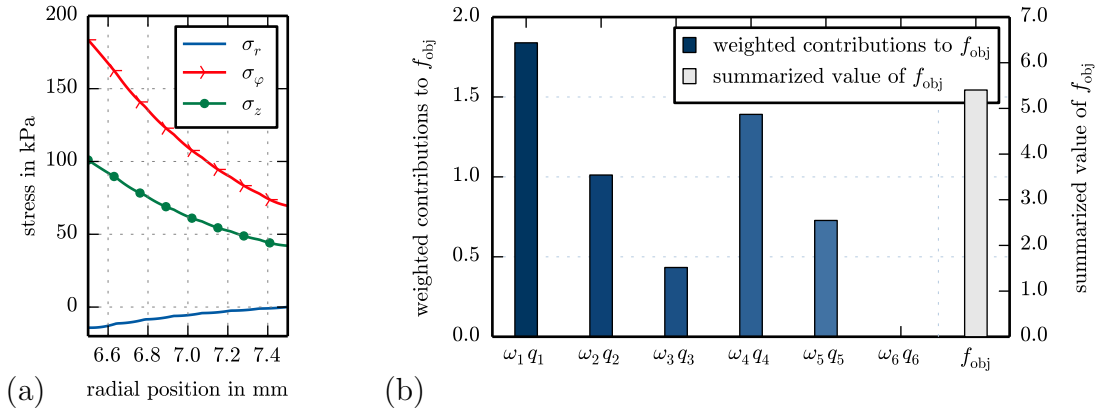
Figure 2: (a) Distribution of the radial, circumferential and axial stresses over the radial position and (b) composition of the value of the objective function in a non-growing pressurized artery with 5 % axial strain.

4.1 Optimization scenarios

For each different combination of $\boldsymbol{F}_\text{g}$-ID and ϕ-ID for different numbers of growth directions n_dir, the limiting values $\vartheta_{(a)}^+$ of the growth factors are identified by minimizing f_obj. In order to also account for different loading scenarios or more specifically, to estimate if a model variant performs insensitive with respect to load changes, the following optimization scenarios are proposed:

1. Optimize $\vartheta_{(a)}^+$ by averaging over different levels of u_z in order to find the best performance over a range of loading situations,

2. Optimize $\vartheta_{(a)}^+$ for a fixed value of u_z in order to find the best performance for a given loading situation,

3. Optimize $\vartheta_{(a)}^+$ and u_z in order to find the best performance of the given growth model over all possible loads.

For the cases where the axial displacement is not an optimization variable, it is chosen among $u_z \in [0.0\,l, 0.1\,l, 0.2\,l]$. For the least sensitive model variant, the value of the objective function obtained in the first case should only minimally differ from the one obtained in the third case. The minimization of the objective function is realized using the "GlobalSearch" algorithm of MATLAB in combination with the solver "fmincon" for constrained nonlinear minimization. Based on preliminary representative numerical calulations, the bounds of the parameters $\vartheta_{(a)}^+$ are chosen as $[1.001, 1.5]$ and the axial displacement is restricted to values within $[0.0\,l, 0.3\,l]$.

4.2 Results and Discussion

Here, the optimization results of some representative model variants are given. Isotropic growth is compared to a series of approaches where three growth directions are included and where the same combination of growth tensor and driving force is considered for each of these directions. An exemplary denomination like "161616" means that $\boldsymbol{F}_{\mathrm{g}}$-ID $= 1$ and ϕ-ID $= 6$ for each of the $n_{\mathrm{dir}} = 3$ parts of the growth tensor. The token "12" denotes isotropic growth, see as well Tables 1 and 2 for explanation of the numbers. For the comparison, a performance measure P is defined as the negative relative deviation of the optimized objective function values with respect to the reference value $f_{\mathrm{obj}}^{\mathrm{ref}} = 5.403$ for the case where no growth and remodeling is included, see Fig. 2 b. Thus, this measure is given by

$$P = -\frac{(f_{\mathrm{obj}} - f_{\mathrm{obj}}^{\mathrm{ref}})}{f_{\mathrm{obj}}^{\mathrm{ref}}}. \tag{11}$$

Higher (positive) values are associated with model variants which indeed lead to stronger improvements in the mechano-biological state. The results for the considered model variants are given in Fig. 3.

For a comprehensive evaluation and discussion, further model variants need to be analyzed and thus, the results given here can only be interpreted as representative examples showing how the proposed methodology for the comparison of different models works. However it can be seen that significantly increased performance measures are observed for anisotropic growth models compared to the purely isotropic formulation. This already indicates that the assumption of isotropic growth may not be realistic as also previously speculated in the literature.
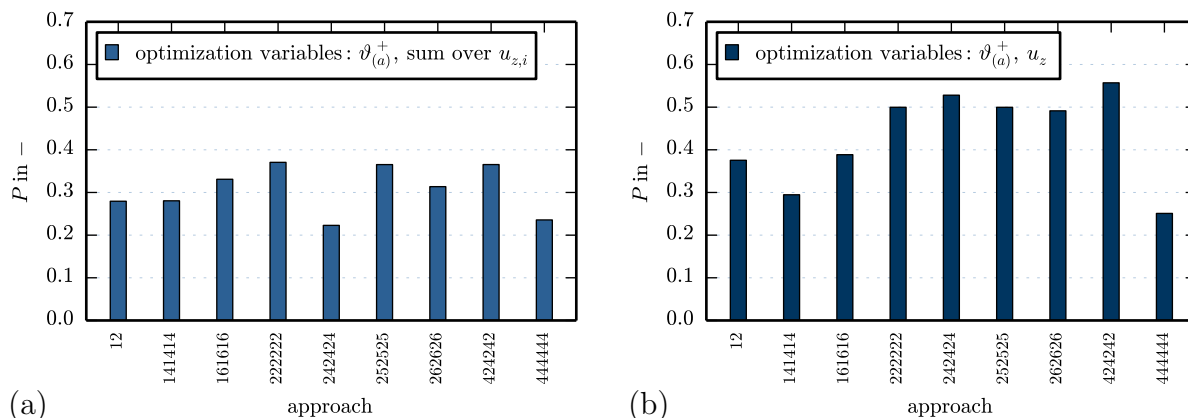
Figure 3: Performance measure P for a subset of different approaches when optimizing (a) the parameters $\vartheta^+_{(a)}$ by averaging over three load levels $u_{z,i}$ or (b) the parameters $\vartheta^+_{(a)}$ and the load level u_z. The tokens on the x-axis are composed of $\boldsymbol{F}_g$-ID and ϕ-ID, consecutively listed for the multiplicative parts of the growth tensor.

5 CONCLUSION

In this contribution, a new method to compare different approaches within an existing framework of combined growth and fiber reorientation in arterial walls was proposed. It relies on the evaluation of a mechano-biologically motivated objective function, which is used to optimize the parameters of different growth models for different loading situations. The objective function is defined at growth equilibrium based on stress peaks, stress inhomogeneities and the volume change due to growth. All these quantities are supposed to be reduced more effectively the better the approach, and hence it might be possible to identify the most realistic growth mechanism. Even though a simplified one-layered model of the artery with a minimized number of optimization variables is used, the results should enable the comparative assessment of the fundamental mechanisms included in the individual model variants. However, only a number of selected variants was analyzed so far and thus, no final conclusion can be drawn with view to which model variant may be most realistic.

6 ACKNOWLEDGEMENT

REFERENCES

[1] Balzani, D.; Neff, P.; Schröder, J. and Holzapfel, G. A. "A polyconvex framework for soft biological tissues. Adjustment to experimental data", *Int. J. Solids Struct.* (2006) **43**:6052–6070.

[2] Balzani, D.; Schröder, J. and Gross, D. "Simulation of discontinuous damage incorporating residual stresses in circumferentially overstretched atherosclerotic arteries",

Acta Biomater. (2006) **2**:609–618.

[3] Brands, D.; Klawonn, A.; Rheinbach, O. and Schröder, J. "Modelling and convergence in arterial wall simulations using a parallel FETI solution strategy", *Comput. Methods Biomech. Biomed. Engin.* (2008) **11**:569–583.

[4] Comellas, E.; Carriero, A.; Giorgi, M.; Pereira, A. and Shefelbine, S. J. "Modeling the influence of mechanics on biological growth", in *Numerical Methods and Advanced Simulation in Biomechanics and Biological Processes* (Eds: M. Cerrolaza, S. J. Shefelbine, D. Garzón-Alvarado), chap. 2, pp. 17–35, Elsevier (2018).

[5] Göktepe, S.; Abilez, O. J. and Kuhl, E. "A generic approach towards finite growth with examples of athlete's heart, cardiac dilation, and cardiac wall thickening", *J. Mech. Phys. Solids* (2010) **58**:1661–1680.

[6] Hariton, I.; deBotton, G.; Gasser, T. C. and Holzapfel, G. A. "Stress-driven collagen fiber remodeling in arterial walls", *Biomech. Model. Mechan.* (2007) **6**:163–175.

[7] Himpel, G.; Kuhl, E.; Menzel, A. and Steinmann, P. "Computational modelling of isotropic multiplicative growth", *Comput. Model. Eng. Sci.* (2005) **8**:119–134.

[8] Holzapfel, G. A.; Gasser, T. C. and Ogden, R. W. "A new constitutive framework for arterial wall mechanics and a comparative study of material models", *J. Elasticity* (2000) **61**:1–48.

[9] Humphrey, J. D. "Cardiovascular Solid Mechanics – Cells, Tissues, and Organs" Springer Science + Business Media (2002), New York.

[10] Kuhl, E.; Maas, R.; Himpel, G. and Menzel, A. "Computational modeling of arterial wall growth. Attempts towards patient-specific simulations based on computer tomography", *Biomech. Model. Mechan.* (2007) **6**:321–331.

[11] Lubarda, V. A. and Hoger, A. "On the mechanics of solids with a growing mass", *Int. J. Solids Struct.* (2002) **39**:4627–4664.

[12] Rodriguez, E. K.; Hoger, A. and McCulloch, A. D. "Stress-dependent finite growth in soft elastic tissues", *J. Biomech.* (1994) **27**:455–467.

[13] Schröder, J. and von Hoegen, M. "An engineering tool to estimate eigenstresses in three-dimensional patient-specific arteries", *Comput. Methods Appl. Mech. Engrg.* (2016) **306**:364–381.

[14] Zahn, A. and Balzani, D. "A combined growth and remodeling framework for the approximation of residual stresses in arterial walls", *Z. Angew. Math. Mech.* (2018) **98**:2072–2100.